APPLIED SCIENCES AND ENGINEERING

Controlled levitation of nanostructured thin films for sun-powered near-space flight

Mohsen Azadi[1], George A. Popov[2], Zhipeng Lu[3], Andy G. Eskenazi[2], Avery Ji Won Bang[1], Matthew F. Campbell[1], Howard Hu[1], Igor Bargatin[1]*

We report light-driven levitation of macroscopic polymer films with nanostructured surface as candidates for long-duration near-space flight. We levitated centimeter-scale disks made of commercial 0.5-micron-thick mylar film coated with carbon nanotubes on one side. When illuminated with light intensity comparable to natural sunlight, the polymer disk heats up and interacts with incident gas molecules differently on the top and bottom sides, producing a net recoil force. We observed the levitation of 6-mm-diameter disks in a vacuum chamber at pressures between 10 and 30 Pa. Moreover, we controlled the flight of the disks using a shaped light field that optically trapped the levitating disks. Our experimentally validated theoretical model predicts that the lift forces can be many times the weight of the films, allowing payloads of up to 10 milligrams for sunlight-powered low-cost microflyers at altitudes of 50 to 100 km.

INTRODUCTION

Currently used flight mechanism cannot be used to achieve sustained flight in Earth's mesosphere—the upper layer of the atmosphere located at altitudes between ~50 and ~80 km (*1*). Modern aircraft are not able to fly for an extended period of time above ~30 to 50 km because the air density at these altitudes is too low to generate lift for airplanes and balloons (*2*–*4*). On the other hand, space satellites rarely dip below ~150 km because the air at such altitudes becomes thick enough to cause excessive drag and heating (*5*, *6*). The only vehicles capable of flying in the mesosphere are rockets, but for only minutes at a time (*1*). We argue below that photophoresis or light-driven motion (*7*–*9*) can potentially provide a no-moving-part mechanism for sustained flight in near space (*1*, *10*).

Recent photophoresis studies have primarily focused on microscopic particles in atmospheric aerosols (*11*–*15*) and the optical trapping of microscopic particles, for example, to create three-dimensional displays (*16*). In the free molecular regime, where the mean free path λ is much larger than the characteristic size a of the object, the photophoretic force results from the difference in the velocity of the incident and departing gas molecules from a hot surface (*17*–*19*). In the continuum regime ($\lambda \ll a$), the force is generated through the thermal creep of the gas over the edges of the sample from the cold side to the hot side (*20*–*23*). The photophoretic force has been shown to reach a maximum in the transition regime, where the Knudsen number $\mathrm{Kn} = \frac{\lambda}{a}$ is of order unity (*24*). In this regime, a mix of free molecular and continuum mechanisms contribute to force generation (*25*), but even at its maximum, the typical value of photophoretic force for a centimeter-sized object is in the micronewton range (*26*). Such low forces constrain the mass of levitatable objects to the milligram range or smaller. At the same time, a substantial temperature difference must typically be generated across a small thickness of such an ultralightweight structure. Recently, we reported hollow nanocardboard plates that have submilligram masses, are thermally insulating enough to generate a few degrees of temperature difference between their top and bottom, and maximize the total photophoretic flow using thousands of microchannels, which was sufficient to levitate such highly engineered structures (*10*, *27*).

However, it is also possible to generate a photophoretic force in ultrathin structures that have a negligible temperature difference but instead have different surface properties on the top and bottom surfaces, as previously demonstrated for micron-sized particles (*28*–*30*). In the free-molecular regime, gas molecules colliding with a heated structure absorb energy from the surface and leave with a higher average speed. The measure for such energy transfer through gas-surface collisions is called the thermal accommodation coefficient, $\alpha = \frac{T_r - T_i}{T_s - T_i}$ (*31*, *32*). Here, T_r is the temperature of reflected gas molecules, and T_i and T_s are incident molecule and structure temperature, respectively. For every combination of a surface material and gas species, there is a unique α, which depends on a variety of factors such as temperature, surface roughness, density, and atomic/molecular weight of the surface and the gas, and even electronic properties of the surface (*33*–*37*). If the thermal accommodation coefficient is larger on the bottom surface of a film than on the top, the gas molecules leave the bottom surface with a higher average velocity compared to the top surface. As a result, the momentum change of the gas molecules and the corresponding recoil of the structure is larger on the bottom side, resulting in a net lift force (Fig. 1A). This type of photophoretic force is generated even if the top and bottom are at identical temperatures, as long as these temperatures are higher than that of the ambient gas.

RESULTS AND DISCUSSION

To demonstrate that this levitation approach can be used not only on the microscopic but also on the macroscopic scale, we fabricated centimeter-scale samples with submicron thickness and different surfaces on the top and bottom. By coating the thinnest commercially available mylar film with carbon nanotubes (CNTs) on only one side (Fig. 1B), we increased the thermal accommodation coefficient on the bottom and generated a photophoretic force that levitated flat disks with centimeter-scale diameters. Notably, these levitating samples can be made using simple fabrication methods from low-cost materials

[1]Department of Mechanical Engineering and Applied Mechanics, University of Pennsylvania, Philadelphia, PA 19104, USA. [2]Vagelos Integrated Program in Energy Research, University of Pennsylvania, Philadelphia, PA 19104, USA. [3]Department of Chemistry, University of Pennsylvania, Philadelphia, PA 19104, USA.
*Corresponding author. Email: bargatin@seas.upenn.edu

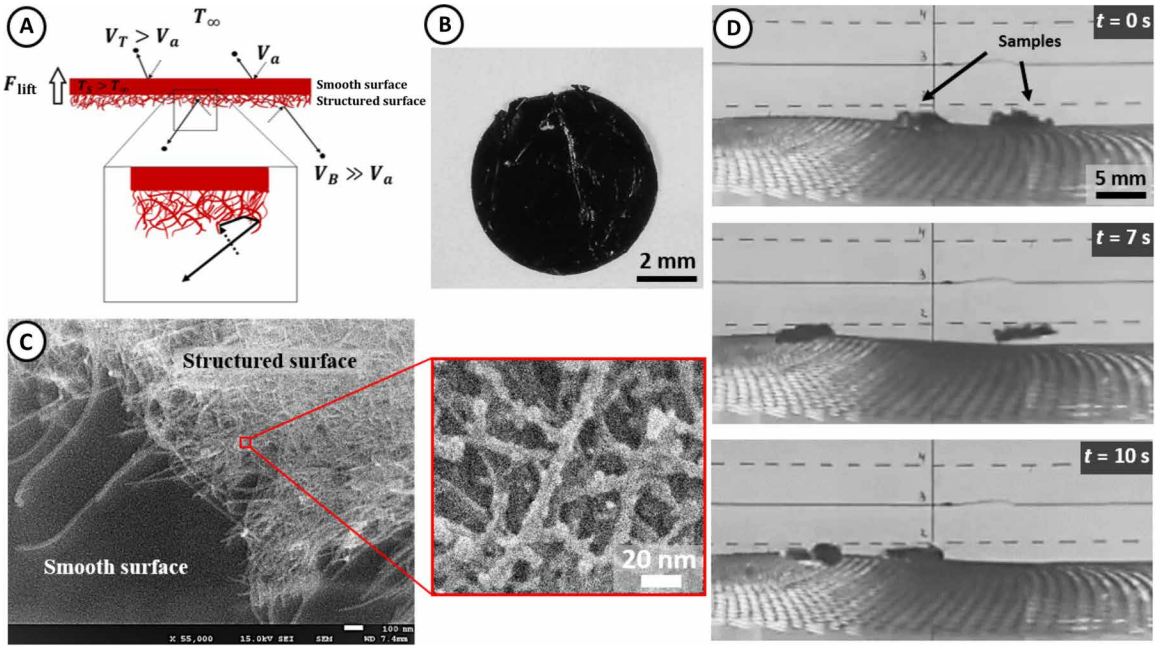

Fig. 1. Force generation mechanism and samples. (**A**) Schematic diagram of the main mechanism behind the photophoretic force due to a difference in the thermal accommodation coefficient (in the free molecular regime). (**B**) Photograph of a 6-mm-diameter mylar disk covered by a layer of CNTs. (**C**) The porous surface of the CNT layer that traps incoming air molecules, allowing for the gas molecules to absorb more heat and approach unity thermal accommodation coefficient partially covering the smooth surface. The inset shows a closeup of the trap created by the nanotubes (**D**) Sequential screenshots of two levitating 6-mm-diameter disks under incident light intensity of $0.5\frac{W}{cm^2}$. Samples placed on a 74% transparent stainless-steel mesh ~6 cm above the light source (movie S1). Photo credit: Mohsen Azadi, University of Pennsylvania.

and achieve stable mid-air hovering at pressures corresponding to altitudes of ~80 km in the atmosphere.

Specifically, we used 500-nm-thick mylar film (also known as OS film in the model airplane community) and deposited a 300-nm-thick layer of CNTs on its bottom side (see Materials and Methods for detail). This layer served three critical functions: (i) to act as a lightweight light absorber with measured visible-range absorptivity of ~90%, (ii) to improve the mylar film's structural rigidity, and (iii) to provide enhanced surface-gas interactions that increase the accommodation coefficient. The areal density of the resulting CNT-coated film was thermal ~1 g/m^2 with an overall thickness of ~0.8 μm. When illuminated by light-emitting diode (LED) arrays with intensity of ~0.5 W/cm^2 (five Suns), the structure became up to ~100 K hotter than the environment (see fig. S2).

The CNT layer has a nanostructured surface shown in Fig. 1C, which tends to trap incoming gas molecules as illustrated in Fig. 1A. These traps make the air molecules collide with the surface multiple times on average before leaving, resulting in a higher thermal accommodation coefficient for the CNT-air side compared to the mylar-air side. This difference between the surface properties results in a higher departing velocity for the air molecules on the CNT (bottom) side compared to the mylar (top) side. The net momentum transfer from these gas-surface interactions results in an upward recoil force that levitates the sample, as shown for the free molecular regime in Fig. 1D (see the Supplementary Materials for the discussion of the force in continuum and transition regimes).

We note that this lift force is not due to the temperature difference between the top and bottom, as in our previous experiments (*10*). Using the thermal conductivity of mylar $k_{mylar} = 0.14\frac{W}{mK}$ and air $k_{air} = 0.025\frac{W}{mK}$ (which is the lower bound for the conductivity of the porous CNT layer), we estimate that the temperature difference is less than $\Delta T_{max} = \frac{I_{light} t_{film}}{2 k_{air}} = 0.1$ K, where $I_{light} = 0.5\frac{W}{cm^2}$ is the typical incident light intensity in our experiments, and $t_{film} \approx 1$ μm is the total thickness of the film and the CNT layer. Since such small temperature differences are insufficient to levitate the film using temperature-driven forces on disks or plates (*10*, *38*) (see the Supplementary Materials for ΔT-force derivation), the observed photophoretic force is not due to the temperature gradient and is instead a result of the difference in the accommodation coefficient of the two sides. We also note that the observed lift force cannot be caused by light (radiation) pressure because the order of magnitude of radiation pressure due to absorption, reflection, or scattering is (*8*) $P_{rad} \sim \frac{I_{light}}{C}$, which for our experimental setup with light intensity of $I_{light} \sim 0.5\frac{W}{cm^2}$ and a disk of 6 mm in diameter results in a net force about three orders of magnitude smaller than the weight of the structures: $F_{rad} = P_{rad} \times \pi r^2 \sim \frac{\pi r^2 I_{light}}{C} = 4.7 \times 10^{-10}$ N $\ll F_{weight} \approx 3 \times 10^{-7}$ N.

To study the force generated by a difference in the thermal accommodation coefficient (Δα-force), we developed a theoretical model and calculated the areal density of an object that can be levitated under a certain flux and a known Δα. Briefly, in the free molecular regime, Δα-force increases proportionally with pressure and reaches a maximum at Knudsen numbers of order unity. Further increases in pressure reduce Δα-force as P^{-2}, which is faster than the P^{-1} scaling that is typical for the temperature difference forces (*20*) (see the Supplementary Materials for full formulation). Our model follows the well-established semi-empirical approach (*8*, *13*, *19*, *24*) to predict the total lift force but not its different components such as area force, edge force, and shear force, which were previously calculated for radiometers (*38*). While the separation of force components can provide additional theoretical insights, such detailed analysis requires

Monte Carlo simulations or numerical solution of the Boltzmann equation, which are computationally demanding and beyond the scope of this study.

Figure 2A shows the predicted areal density of an object that can be levitated using Δα-force with Δα = 0.15 ± 0.05 and flux of ~0.5 $\frac{W}{cm^2}$ (~5 times the direct sunlight intensity on the surface of Earth and ~4 times the direct sunlight intensity in the upper atmosphere) as well as the results of our experiments with the CNT-covered mylar disk. This value of Δα = 0.15 ± 0.05 was found by fitting the theoretical predictions of successful levitation to experimental results (see fig. S5) and is in good agreement with the typical Δα difference reported in the literature between rough and smooth surfaces of photophoretically levitating microscopic particles (*13*). Figure 2B compares the pressure-dependent lift force to the weight of the 6-mm-diameter sample, with upward and downward arrows indicating levitation and no levitation, respectively, in experiments. We note that the operational range of our mylar samples was limited by the maximum temperature of ~400 K they could sustain before noticeable curling deformation (movie S5 and fig. S2B). This temperature threshold was then used to map the operational range in Fig. 2, which agrees with the experiments. Below these temperatures, we only see a small edge deformation with radii of curvature much smaller than the radius of the disk. Such local edge deformations do not significantly affect the absorbed light power or the lift force (Fig 3B).

To levitate samples for extended periods of time, we designed a light field that can optically trap the sample. This light trap consisted of a central area with intensity high enough to levitate the disk, surrounded by a ring of even higher intensity, which creates a restoring force by tilting the disk and pushing back toward the center (Fig. 3). The uneven light field also creates a ΔT-shear force (*35*) that points in the same direction. Determining which restoring mechanism is dominant in our experiments is complicated and is beyond the scope of this study.

Considering the dimensions and thermal properties of the sample material, the thermalization time constant can be estimated as $\tau = \frac{\rho_{Mylar} C_{disk} V_{disk}}{h_{total} A_{disk}} = \frac{\rho_{disk} C_{disk} t_{disk}}{2 h_{total}} \sim 0.04$ s, where $\rho_{Mylar} = 1390 \frac{kg}{m^3}$, $C_{Mylar} = 1170 \frac{J}{kg\,K}$, $t_{disk} = 0.8$ μm as the density, heat capacity, and effective thickness of the disk, $A_{disk} = 2\pi a^2$ is the total area, V_{disk} is the volume of the disk, and $h_{total} = \frac{Q_{tot}}{A_{disk}(T_s - T_{amb})}$ is the average heat transfer coefficient from the disk to the ambient and found numerically (see the Supplementary Materials). For the successful experiments shown in Fig. 3A, $h_{total} \sim 17 \frac{W}{m^2 K}$. When the incident light is kept at a constant intensity, the sample reaches thermal equilibrium after a few time constants or about 0.1 s. Therefore, the light trap needs to be wide enough that the thermalization and the restoring force occur before the disk can cross the high-intensity ring, escaping from the trap. We used two light traps to study this effect. The first consisted of four high-intensity arrays of LEDs placed in a square pattern, creating a light ring of ~4 cm in diameter, which proved insufficient since the initial liftoff speed would push the samples out of the trap very quickly, before thermalization (see movie S4). The second setup had eight high-intensity arrays of LEDs arranged in a ring pattern with a diameter of about 15 cm shown in Fig. 3B. We also observed the samples levitate when the light was shone from above, demonstrating that this levitation mechanism can work for any direction of the incident light because the mylar film is optically transparent (movie S6). However, creating a trapping beam configuration is more complex when illuminating from above and we did not pursue it.

Several tests using side and oblique video recording revealed that the light trap was effective, and the samples levitated at a height comparable to their diameter above the mesh (see movies S1 to S3). This equilibrium height is determined by the intensity of light the samples receive as a function of the distance from the LEDs. The samples stay levitated at a height where the light received generates a force that exactly balances their weight. After several seconds of successful levitation, we typically increased the light intensity at a rate of ~0.3 $\frac{W}{cm^2}$ per minute to increase the levitation height, which, however, also resulted in a gradual temperature increase that slowly deformed the

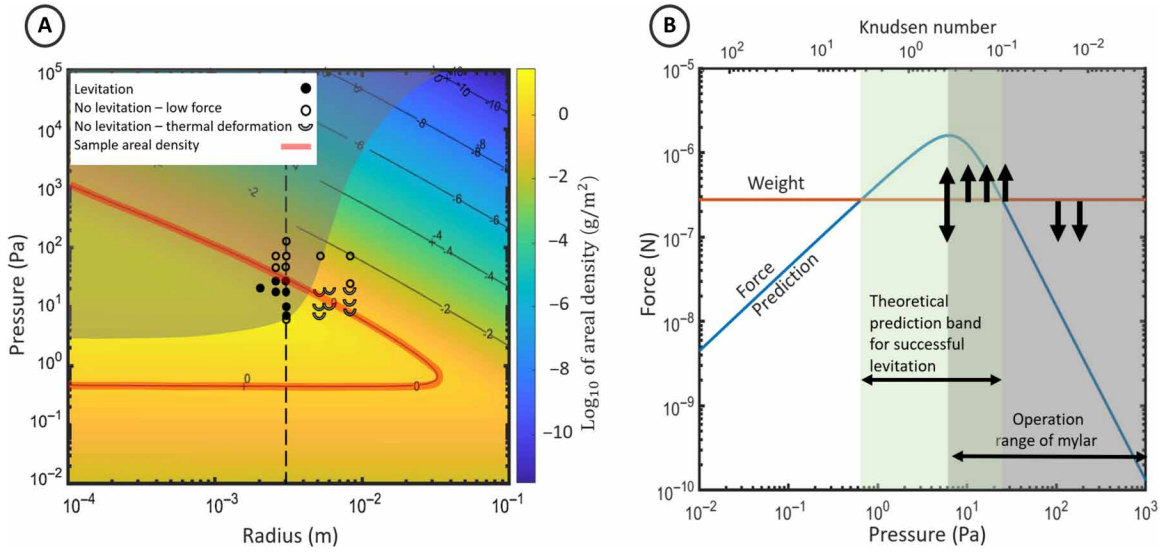

Fig. 2. Experimental data and theoretical prediction. (**A**) Areal density of a disk with a given radius and micron thickness that can be levitated under 0.5 $\frac{W}{cm^2}$ and Δα = 0.15. The shaded area represents the domain that mylar can operate without undergoing thermal deformation due to temperatures exceeding 400 K (see the Supplementary Materials). (**B**) Comparison of the force and weight for a disk with 6-mm diameter with thermal deformation considerations (the size corresponding to the dashed line in Fig. 2A).

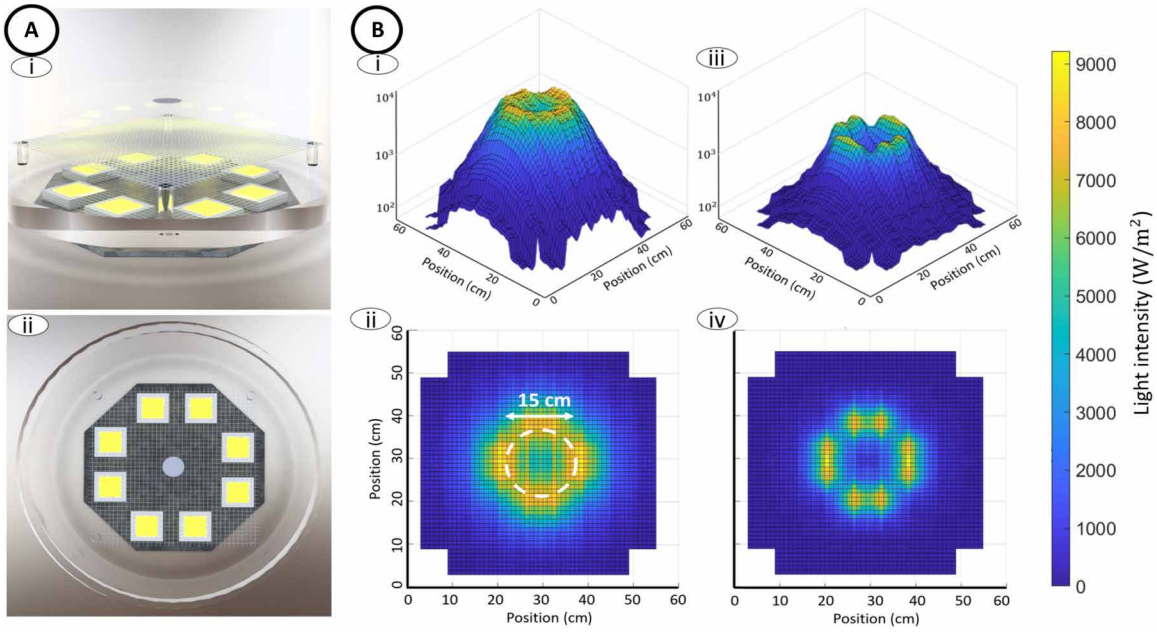

Fig. 3. Optical trap configuration. (**A**) (i) Side and (ii) top-view schematic diagram of the test setup consisting of eight LED arrays below an acrylic vacuum chamber, a 74% transparent metallic mesh placed several centimeters above the bottom surface of the acrylic chamber and a levitating disk sample. (**B**) Experimental measurements of the intensity of the trapping light beam from eight LED arrays at 7-cm (i and ii) and 10-cm (iii and vi) heights above the LEDs. Note that the high-intensity ring surrounding the microflyer confines its in-plane movement and that the intensity at the center drops as the height increases, which stabilizes the flight height.

sample after approximately 30 s. Once deformed, the lift force was reduced and a random side force appeared, occasionally pushing it outside of the light trap. (The presence of these side forces also suggests a possible future mechanism by which the disks could be steered in mid-air by controllably changing the shape of the structure.) In most cases, the deformation also resulted in a lower effective light-absorbing area, which then caused the sample to gradually settle down within the light trap. At lower intensities or for stiffer disks, we expect the structures to remain in the light trap indefinitely.

Using our model for the photophoretic force on a disk, we can predict the possibility of photophoretic flight at different altitudes in the atmosphere. As the altitude increases from 0 to 100 km, ambient temperature and pressure change markedly (see the Supplementary Materials and fig. S4), which affects the temperature difference between the disk and ambient. In our model, we also accounted for different radiation environments seen by the top and bottom of the disk at altitudes above 30 km. Conservatively, we assumed a 3 K effective temperature for deep space, seen by the top side of the disk, and 255 K for Earth, seen by the bottom side (*39*).

As shown in Fig. 4, our theoretical model predicts the possibility of sunlight-powered levitation in a wide range of altitudes between 50 and 100 km if the accommodation coefficient of the surfaces can reach $\Delta\alpha = 0.5$ and the thermal infrared emissivity is reduced to $\epsilon = 0.5$. Moreover, the disks can lift up to 10 mg of payload under natural sunlight, sufficient to carry smart dust sensors presented in the literature (*40*). Thermal accommodation coefficient value for air on clean glass and air on glass coated with molecularly thin polymer is reported to be 0.19 and 0.43, respectively (*41*), which means that $\Delta\alpha = 0.5$ is realistic with carefully treated surfaces. The use of selective absorbers has been shown to reduce the emissivity to as low as $\epsilon \sim 0.1$ (*42*), which would allow levitation even for incident light intensities below full natural sunlight intensity (see fig. S9). At high altitudes (>20 km), the sunlight intensity is approximately $0.136 \frac{W}{cm^2}$ for normal incidence. We note, however, that the absorbed power can be another 30% larger because the disks will also absorb sunlight reflected from Earth (assuming albedo of ~0.3). Because of low ambient temperatures at high altitudes, the disk temperature can remain below 400 K (Fig. 4C), allowing the use of mylar or other polymer materials without thermal deformation.

To prevent the tumbling of the microflyer due to winds or other disturbances at high altitudes, the payload can be suspended by, e.g., a carbon fiber thread from the disk to lower its center of mass and suppress the tilting of the sample. Moreover, controllable tilting and horizontal movement of the samples can be achieved in such structures by shifting the position of the payload along the thread that suspends the payload from the disk. Another possibility for further improvement of payload capacity is using an array of microflyers, with potentially hundreds of microflyers connected by ultrathin carbon fibers, which can potentially increase the payload into the gram range.

In summary, this work demonstrated an approach to photophoretic levitation of macroscopic structures that does not require a temperature gradient within the object, offering a path to the development of affordable photophoretic microflyers for the mesosphere. We developed a theoretical model for thin disks, which showed agreement with the experiments done using low-cost fabrication methods. The levitation tests were successful at pressures of ~10 Pa and incident light intensity of $0.5 \frac{W}{cm^2}$. We also presented a method to trap and control the hovering of the thin microflyers. Last, photophoretic levitation through $\Delta\alpha$-force showed consistent upward lift force direction regardless of the direction of incoming light.

Our experimentally validated model predicts that the same approach can be used in the near space at altitudes between 50 and

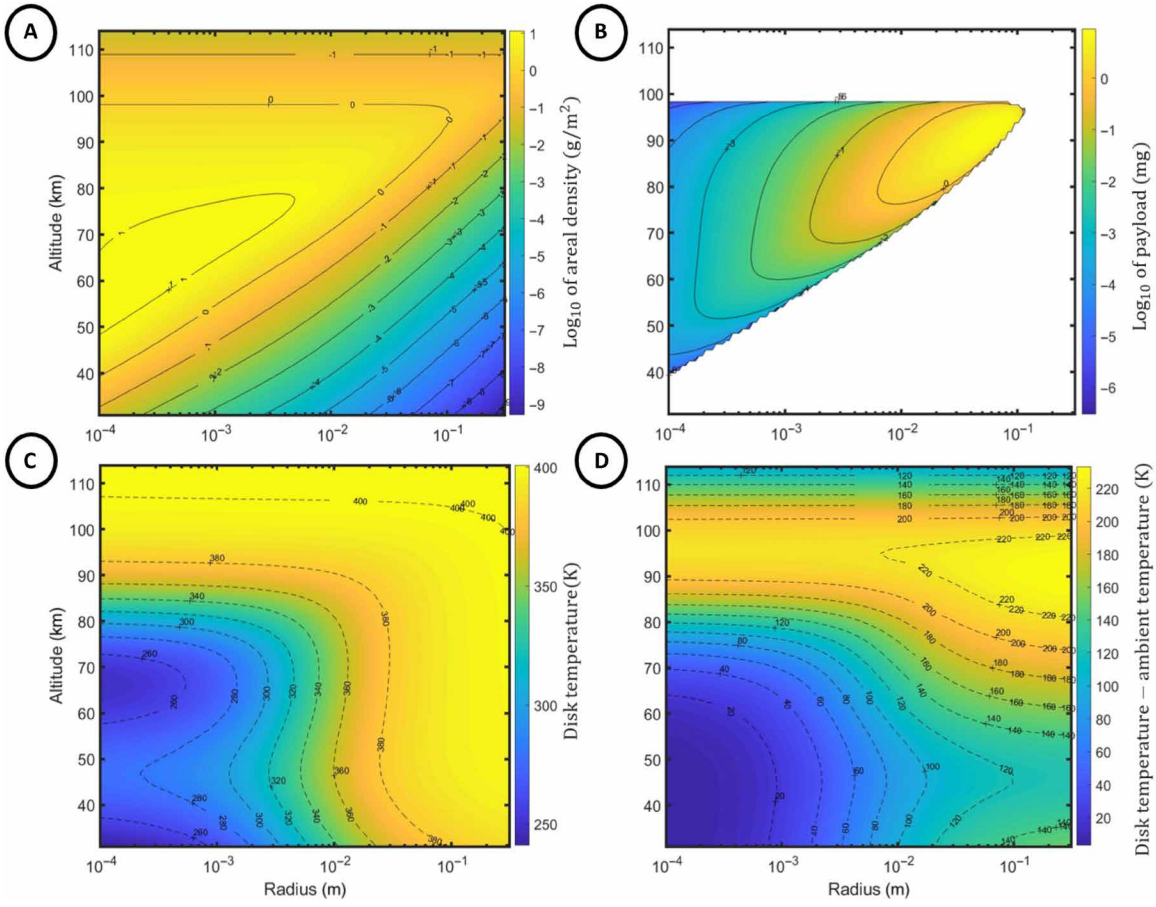

Fig. 4. Near-space flight prediction. Contour plots of (**A**) areal density of the object able to be levitated (**B**) payload that can be lifted using mylar-CNT (white area represents no levitation for mylar areal density). (**C**) Temperature and (**D**) temperature difference between the disk and ambient for different sizes at different altitudes with $\Delta\alpha = 0.5$, $\epsilon = 0.5$, and under natural sunlight $\left(0.136\frac{W}{cm^2}\right)$.

100 km. Such microflyers can use sunlight or a laser beam from any direction to stay levitated for extended periods of time, allowing, for example, the mapping of wind flows at these high altitudes by tracking the location of these flyers using a radar or lidar. There is a large opportunity to further increase the force by increasing the difference in accommodation coefficients and reducing the infrared emissivity. Such improvements will allow the microflyers to carry payloads of up to 10 mg, which can consist of thin substrate or smart dust sensors for weather and climate applications, such as measuring temperature, pressure, or carbon dioxide levels.

MATERIALS AND METHODS

Sample fabrication process

We started with a thin sheet of commercially available mylar film with a nominal thickness of 0.5 μm (Dupont). Using a 1-cm^2 sample and a precision scale (PerkinElmer AD4 model), we measured the areal density to be ~0.7 g/m^2, which agrees with the theoretical value expected from the nominal density of mylar of 1.39 kg/m^3. To deposit the CNT layer, we used a 0.2 weight % water-based single-wall CNT with 1- to 2-nm diameter and 5- to 30-μm length (NanoAmor) and diluted it with deionized (DI) water by a volumetric ratio of 3:1 (DI Water/CNT). We then stretched a sheet of this mylar thin film of a Si wafer and put it on a hot plate at 50°C. By dropcasting the CNT solution on the sheet and letting the water evaporate, we created a CNT layer on the mylar sheet, then peeled the mylar sheet off of the Si substrate, and cut circular samples of the desired diameter using a razor blade. Weight measurements of the CNT-covered samples showed their areal density to be ~1 g/m^2.

Testing methods

The experimental setup used a 10-liter custom-designed cylindrical acrylic vacuum chamber. The acrylic allowed for easy illumination of the sample from any direction and allows for video capture from any direction. Despite the 25-mm thick walls and properly sealed junctions, the chamber leaked a substantial amount of air through its walls (a known downside of acrylic chambers), making it impossible to reach high-vacuum base pressures. A two-stage vacuum pump with a 1500-Hz turbo pump resulted in base pressures ranging from 7 to 200 Pa (~0.05 to 1.5 torr) by using the roughing-turbo combination or only the roughing pump.

To create a light trap that has a local minimum in the center and a ring of maximum intensity, we used eight LED arrays, each rated for 100 W of input power (LOHAS LH-XP-100W-6000k). These LEDs, as shown in fig. S1, were mounted on two pieces of aluminum connected to four heat sinks with forced convection cooling from four fans, capable of removing ~1000 W in total. All thermal interfaces were enhanced using silver paste (Arctic Silver 5 Polysynthetic Thermal

Compound). In all experiments, a metallic mesh with a transparency of 74% (McMaster item no. 9238T51) was used as a "launchpad" and was placed several centimeters away from any inner surface of the vacuum chamber to avoid ground or wall effects. Figure S1 shows a side view of the chamber, the eight-LED-array assembly, and the launchpad. To study the residual ground effect of the launchpad, we also created and tested an 85% transparent mesh by removing approximately one half of the wires of the 74% mesh. The experimental results showed no measurable difference in the height versus input power to the LEDs, suggesting that the effect of the mesh is negligible.

SUPPLEMENTARY MATERIALS

Supplementary material for this article is available at http://advances.sciencemag.org/cgi/content/full/7/7/eabe1127/DC1

REFERENCES AND NOTES

1. M. Young, S. Keith, A. Pancotti, An overview of advanced concepts for near-space systems, in 45th AIAA/ASME/SAE/ASEE Joint Propulsion Conference & Exhibit (2009), Denver, Colorado, 2 to 5 August 2009.
2. J. A. Drezner, R. S. Leonard, *Innovative Development: Global Hawk and Darkstar - Flight Test in the HAE UAV ACTD Program* (RAND Corporation, 2002).
3. L. J. Ehernberger, C. Donohue, E. H. Teets, A review of solar-powered aircraft flight activity at the pacific missile range test facility, Kauai, Hawaii, in 11th Conference on Aviation, Range, and Aerospace (2004), Hyannis, MA, 3 October 2004.
4. S. Smith, M. Fortenberry, M. Lee, R. Judy, The HiSentinel Airship (2007).
5. A. J. Knoedler, Lowering the high ground: Using near-space vehicles for persistent C3ISR. Center for Strategy and Technology, Air War College, Air University (2005).
6. J. Laštovička, R. A. Akmaev, G. Beig, J. Bremer, J. T. Emmert, Global change in the upper atmosphere. *Science* **314**, 1253–1254 (2006).
7. O. Jovanovic, Photophoresis—Light induced motion of particles suspended in gas. *J. Quant. Spectrosc. Radiat. Transf.* **110**, 889–901 (2009).
8. H. Horvath, Photophoresis – a forgotten force ?? *KONA* **31**, 181–199 (2014).
9. S. Dong, Y. Liu, Investigation on the photophoretic lift force acting upon particles under light irradiation. *J. Aerosol Sci.* **113**, 114–118 (2017).
10. J. Cortes, C. Stanczak, M. Azadi, M. Narula, S. M. Nicaise, H. Hu, I. Bargatin, Photophoretic levitation of macroscopic nanocardboard plates. *Adv. Mater.* **32**, 1906878 (2020).
11. N. T. Tong, Experiments on photophoresis and thermophoresis. *J. Colloid Interface Sci.* **51**, 143–151 (1975).
12. M. Kerker, D. D. Cooke, Photophoretic force on aerosol particles in the free-molecule regime. *J. Opt. Soc. Am.* **72**, 1267–1272 (1982).
13. H. Rohatschek, Photophoresis and accommodation, *Optika Atmosfery i Okeana*, 27, 87–96 (2014); http://sibran.ru/upload/iblock/4ac/4ac3c7765d39af09f4672d2522ed9f6a.pdf [retrieved 20 May 2020].
14. A. A. Cheremisin, I. S. Shnipov, H. Horvath, H. Rohatschek, The global picture of aerosol layers formation in the stratosphere and in the mesosphere under the influence of gravito-photophoretic and magneto-photophoretic forces. *J. Geophys. Res.* **116**, D19204 (2011).
15. D. W. Keith, Photophoretic levitation of engineered aerosols for geoengineering. *Proc. Natl. Acad. Sci. U.S.A.* **107**, 16428–16431 (2010).
16. D. E. Smalley, E. Nygaard, K. Squire, J. Van Wagoner, J. Rasmussen, S. Gneiting, K. Qaderi, J. Goodsell, W. Rogers, M. Lindsey, K. Costner, A. Monk, M. Pearson, B. Haymore, J. Peatross, A photophoretic-trap volumetric display. *Nature* **553**, 486–490 (2018).
17. W. Zulehner, H. Rohatschek, Photophoresis of nonspherical bodies in the free molecule regime. *J. Colloid Interface Sci.* **138**, 555–564 (1990).
18. S. Tehranian, F. Giovanie, J. Blum, Y. Xu, B. Å. S. Gustafson, Photophoresis of micrometer-sized particles in the free-molecular regime. *Int. J. Heat Mass Transf.* **44**, 1649–1657 (2001).
19. C. Loesche, G. Wurm, T. Jankowski, M. Kuepper, Photophoresis on particles hotter/colder than the ambient gas in the free molecular flow. *J. Aerosol Sci.* **97**, 22–33 (2016).
20. L. D. Reed, Low Knudsen Number photophoresis. *J. Aerosol Sci.* **8**, 123–131 (1977).
21. A. B. Pluchino, Photophoretic force on particles for low Knudsen number. *Appl. Optics* **22**, 103–106 (1983).
22. M. M. R. Williams, Thermophoretic forces acting on a spheroid. *J. Phys. D Appl. Phys.* **19**, 1631–1642 (1986).
23. C. L. Ou, H. J. Keh, Low Knudsen number photophoresis of aerosol spheroids. *J. Colloid Interf. Sci.* **282**, 69–79 (2005).
24. H. Rohatschek, Semi-empirical model of photophoretic forces for the entire range of pressures. *J. Aerosol Sci.* **26**, 717–734 (1995).
25. C. Loesche, T. Husmann, Photophoresis on particles hotter/colder than the ambient gas for the entire range of pressures. *J. Aerosol Sci.* **102**, 55–71 (2016).
26. N. T. Tong, Photophoretic force in the free molecule and transition regimes. *J. Colloid Interface Sci.* **43**, 78–84 (1973).
27. C. Lin, S. M. Nicaise, D. E. Lilley, J. Cortes, P. Jiao, J. Singh, M. Azadi, G. G. Lopez, M. Metzler, P. K. Purohit, I. Bargatin, Nanocardboard as a nanoscale analog of hollow sandwich plates. *Nat. Commun.* **9**, 4442 (2018).
28. H. Rohatschek, Direction, magnitude and causes of photophoretic forces. *J. Aerosol Sci.* **16**, 29–42 (1985).
29. J. Lin, A. G. Hart, Y. Li, Optical pulling of airborne absorbing particles and smut spores over a meter-scale distance with negative photophoretic force. *Appl. Phys. Lett.* **106**, 171906 (2015).
30. G. Chen, L. He, M. Wu, Y. Li, Temporal dependence of photophoretic force optically induced on absorbing airborne particles by a power-modulated laser. *Phys. Rev. Appl.* **10**, 054027 (2018).
31. L. B. Thomas, R. C. Golike, A comparative study of accommodation coefficients by the temperature jump and low-pressure methods and thermal conductivities of He, Ne, and CO_2. *J. Chem. Phys.* **22**, 300 (1954).
32. F. O. Goodman, Thermal accommodation coefficients. *J. Phys. Chem.* **84**, 1431–1445 (1980).
33. D. M. Gilbey, A re-examination of thermal accommodation coefficient theory. *J. Phys. Chem. Solid* **23**, 1453–1461 (1962).
34. P. Feuer, Theory of the thermal accommodation coefficients of a diatomic gas. *J. Chem. Phys.* **39**, 1311–1316 (1963).
35. F. O. Goodman, H. Y. Wachman, Formula for thermal accommodation coefficients. *J. Chem. Phys.* **46**, 2376–2386 (1967).
36. W. M. Trott, D. J. Rader, J. N. Castañeda, J. R. Torczynski, M. A. Gallis, Measurement of gas-surface accommodation. *AIP Conf. Proc.* **1084**, 621 (2008).
37. M. Grau, F. Völklein, A. Meier, C. Kunz, J. Heidler, P. Woias, Method for measuring thermal accommodation coefficients of gases on thin film surfaces using a MEMS sensor structure. *J. Vac. Sci. Technol. A* **34**, 041601 (2016).
38. A. Ketsdever, N. Gimelshein, S. Gimelshein, N. Selden, Radiometric phenomena: From the 19th to the 21st century. *Vacuum* **86**, 1644–1662 (2012).
39. D. Hartmann, *Global Physical Climatology* (Elsevier Science, ed. 2, 2015).
40. Y. Lee, S. Bang, I. Lee, Y. Kim, G. Kim, M. H. Ghaed, P. Pannuto, P. Dutta, D. Sylvester, D. Blaauw, A modular 1 mm^3 die-stacked sensing platform with low power I^2C inter-die communication and multi-modalt energy harvesting. *IEEE J. Solid State Circuits* **48**, 229–243 (2013).
41. C. D. F. Honig, W. A. Ducker, Effect of molecularly-thin films on lubrication forces and accommodation coefficients in air. *J. Phys. Chem. C.* **114**, 20114–20119 (2010).
42. K. Xu, M. Du, L. Hao, J. Mi, Q. Yu, S. Li, A review of high-temperature selective absorbing coatings for solar thermal applications. *J. Materiomics* **6**, 167–182 (2020).
43. Y. A. Çengel, M. A. Boles, *Thermodynamics: An Engineering Approach* (McGraw-Hill, 2001).
44. E. W. Lemmon, R. T. Jacobsen, Viscosity and thermal conductivity equations for nitrogen, oxygen, argon, and air. *Int. J. Thermophys.* **25**, 21–69 (2004).
45. F. S. Sherman, *Rarefied Gas Dynamics*, J. A. Laurman, Ed. (Academic Press, 1963), vol. 2, p. 228.
46. C. V. Madhusudana, *Thermal Contact Conductance* (Springer, 2014).
47. A. V. Filippov, D. E. Rosner, Energy transfer between an aerosol particle and gas at high temperature ratios in the Knudsen transition regime. *Int. J. Heat Mass Transf.* **43**, 127–138 (2000).
48. M. M. Yovanovich, *On the Effect of Shape, Aspect Ratio and Orientation Upon Natural Convection from Isothermal Bodies of Complex Shape* (ASME Winter Annual Meeting, Boston, MA, 1987).
49. M. Knudsen, S. Weber, Luftwiderstand gegen die langsame Bewegung kleiner Kugeln. *Ann. Physik* **341**, 981–994 (1911).
50. E. H. Kennard, *Kinetic Theory of Gases* (McGraw-Hill, New York, 1938).
51. R. S. Alassar, Heat conduction from spheroids. *J. Heat Transfer* **121**, 497–499 (1999).
52. R. Černý, F. Vodák, A theoretical relation between viscosity and thermal conductivity of gases based on macroscopic balance equations. *Czech J. Phys.* **44**, 913–926 (1994).
53. S. G. Jennings, The mean free path in air. *J. Aerosol Sci.* **19**, 159–166 (1988).
54. R. N. Barshinger, J. F. Geer, Stokes flow past a thin oblate body of revolution: Axially incident uniform flow. *SIAM J. Appl. Math.* **44**, 19–32 (1984).
55. D. J. Jacob, *Introduction to Atmospheric Chemistry* (Princetonre Univ. Press, 1999); http://acmg.seas.harvard.edu/people/faculty/djj/book/bookchap2.html, Chapter 2.

Acknowledgments: We thank the staff of the Singh Center for Nanotechnology, Nanoscale Characterization Facility, and Scanning and Local Probe facility at the University of

Pennsylvania. **Funding:** The Singh Center for Nanotechnology, Nanoscale Characterization Facility, and Scanning and Local Probe facility at the University of Pennsylvania is partly funded by the NSF National Nanotechnology Coordinated Infrastructure Program, under grant NNCI-1542153. This work is partly supported by the NSF under CBET-1845933 and the School of Engineering and Applied Science at the University of Pennsylvania. **Author contributions:** The experimental samples were fabricated by M.A. and G.A.P. Experimental testing and characterization was performed by M.A., G.A.P., Z.L., and A.G.E. Theoretical models were developed by M.A., H.H., and I.B. Numerical simulations were performed by M.A. and A.J.W.B. The project was conceived and directed by I.B. The manuscript was written by M.A., M.F.C., and I.B. with contributions from all authors. **Competing interests:** The authors declare that they have no competing interests. **Data and materials availability:** All data needed to evaluate the conclusions in the paper are present in the paper and/or the Supplementary Materials. Additional data related to this paper may be requested from the authors.

Submitted 31 July 2020
Accepted 24 December 2020
Published 12 February 2021
10.1126/sciadv.abe1127

Citation: M. Azadi, G. A. Popov, Z. Lu, A. G. Eskenazi, A. J. W. Bang, M. F. Campbell, H. Hu, I. Bargatin, Controlled levitation of nanostructured thin films for sun-powered near-space flight. *Sci. Adv.* **7**, eabe1127 (2021).

Science Advances

Controlled levitation of nanostructured thin films for sun-powered near-space flight

Mohsen Azadi, George A. Popov, Zhipeng Lu, Andy G. Eskenazi, Avery Ji Won Bang, Matthew F. Campbell, Howard Hu and Igor Bargatin

Sci Adv **7** (7), eabe1127.
DOI: 10.1126/sciadv.abe1127